High temperature oxidation of NiCrAlY coated Alloy 625 manufactured by selective laser melting

Damien Texier, Etienne Copin, Augustin Flores, Jiwon Lee, Mathieu Terner, Hyun-Uk Hong, Philippe Lours

High temperature oxidation of NiCrAlY coated Alloy 625 manufactured by selective laser melting

Damien Texier[a,*], Etienne Copin[a], Agustin Flores[a], Jiwon Lee[a,b], Mathieu Terner[b], Hyun-Uk Hong[b], Philippe Lours[a]

[a] Institut Clement Ader (ICA) - UMR CNRS 5312, Université de Toulouse, CNRS, INSA, UPS, Mines Albi, ISAE-SUPAERO, Campus Jarlard, 81013 Albi Cedex 09, France
[b] Department of Materials Science and Engineering, Changwon National University, 20 Changwondaehak-ro, Changwon, Gyeongnam 51140, Republic of Korea

Keywords:
MCrAlY bond-coating
Superalloy
Additive manufacturing
Selective laser melting
Oxidation
Dilution

A B S T R A C T

The high temperature oxidation of fully SLM-processed NiCrAlY coated Alloy 625 parts was investigated between 800 °C and 1000 °C. For comparison, bulk NiCrAlY and bulk Alloy 625 were also fabricated using SLM. Two thin layers of NiCrAlY powder were lasered at the surface of Alloy 625 to form the bi-materials. Bulk NiCrAlY and bi-materials showed an improved oxidation behavior compared to Alloy 625. The oxidation of the NiCrAlY coating results in regions with a dense and continuous external Al_2O_3 layer and regions composed of a mixture of external Cr_2O_3 and internal Al_2O_3. Large EDS maps at the surface and cross-sections of the bi-material highlighted a heterogeneous distribution of constitutive elements of the NiCrAlY coating, resulting in some regions with an Al activity lower than the one required for the formation of a continuous and dense Al_2O_3 layer ($\leq$10 atomic percent). Low Al activity and high Al activity regions were related to the topography of the SLMed surface and correspond to hill and valley regions, respectively. In addition, cracks, mainly occurring in high Al activity regions, were observed across NiCrAlY specimens. The fabrication of coated but small components with a brittle coating by SLM is not trivial and needs further investigations.

1. Introduction

Nickel-based superalloys are intensively used in the aerospace industry for high temperature applications because of their excellent mechanical strength combined with their resistance to high temperature oxidation and corrosion [1–3]. Alloy 625, consisting of a Ni base FCC γ-Ni matrix solution strengthened by significant additions of Cr, Nb and Mo, was purposely developed to achieve an interesting trade-off between mechanical strength, fracture toughness, weldability, manufacturing and corrosion/oxidation performance under aggressive environments [4–8]. Its good resistance to high temperature surface reactivity derives from the considerable amount of chromium present in the alloy, *i.e.* about 20% in weight and 24 atomic %, promoting the formation of a continuous and protective external Cr_2O_3 oxide layer and internal Al_2O_3 oxides in a large temperature window [5,9–12]. Alloy 625 exhibits a parabolic oxidation behavior between 600 °C and 1050 °C [9]. The parabolic constant of oxidation follows an Arrhenius relation with a frequency factor k_0 of $8.3.10^{-2} \pm 2.7\ g^2.cm^{-4}.s^{-1}$ and an activation energy Q of $232 \pm 11\ kJ.mol^{-1}$ regardless of the partial pressure of oxygen between 0.12 and 10.3 kPa in the 1050 °C–1250 °C temperature range [9]. Above 1050 °C, Nb and Ti are found in the upper regions of the oxide scale and a slight decrease in oxidation rate is noticed as a function of the exposure time. This could be caused by either changes in the oxide-film composition or by the possible volatilization of Cr_2O_3 due to the formation of the CrO_3 (g) compound [13]. Cr_2O_3 volatilization is accelerated with the increase in temperature, in partial pressure of oxygen or in the presence of water [13,14]. Both the chromium depletion associated with the formation of Cr_2O_3 and its volatilization impair the subsurface microstructure and the high temperature structural performance of Alloy 625. Such an oxidation-assisted degradation of component integrity is particularly harmful for small-size and/or thin structural components. Therefore, improvement in surface reactivity of Alloy 625 at high temperature is of high interest. High temperature protective coatings, such as aluminide diffusion coatings or MCrAlY overlay coatings, are commonly used onto nickel-based superalloys to promote the formation of dense and very low-growth-rate α-Al_2O_3 and/or Cr_2O_3 oxide scale [15–18]. The improvement in high temperature oxidation properties above 1000 °C of NiCrAlY coatings containing more than 10 atomic % of aluminum was demonstrated from decades due to the formation and growth of a

* Corresponding author.
E-mail address: damien.texier@mines-albi.fr (D. Texier).

Table 1
Nominal composition of the Alloy 625 and NiCrAlY powders used for SLM manufacturing measured by ICP-OES (in % at.), and composition range for bulk Alloy 625, bulk NiCrAlY and NiCrAlY coated Alloy 625 measured by EDS (in % at.).

Element	Ni	Cr	Mo	Fe	Co	C	Nb	Al	Y
Alloy 625 (powder)	Bal.	22.9	5.10	3.70	0.60	0.39	1.99	0.76	–
NiCrAlY (powder)	Bal.	21.9	–	–	–	–	–	17.9	0.7
Bulk Alloy 625 (SLM)	Bal.	23–25	5–6	3–5	0.5–0.7	–	1.7–2.3	0.5–1.5	–
Bulk NiCrAlY (SLM)	Bal.	18–25	–	–	–	–	–	17–21	0.2–0.5
NiCrAlY Coating (SLM)	Bal.	21–24	3–5	0.3–0.6	–	–	2–3	3–12	0.1–0.3

continuous, compact, and adherent α-Al_2O_3 [19–21]. However, the oxidation performance of NiCrAlY alloys below 1000 °C could be significantly impaired, and can be even worse than Alloy 625 in terms of mass evolution [22–24]. This change in oxidation behavior is attributed to the growth of other Al_2O_3 allotropic variants, *i.e.* θ-Al_2O_3 and γ-Al_2O_3, showing higher oxidation kinetics, and/or the growth of external Cr_2O_3. Therefore, improving the oxidation resistance of Alloy 625 using NiCrAlY coatings for temperature lower than 1000 °C is of high interest, but not straightforward.

The need for improved performance while satisfying both structural and environmental specifications leads to more and more complex design in terms of geometry and multi-layered microstructures for high temperature jet engine and power plant turbines. Conventional manufacturing processes, such as forging, casting and/or powder metallurgy can find limitations for highly complex geometries, integrated structures, miniaturized and/or small-volume production. Additive manufacturing (AM) techniques are nowadays particularly appropriate for manufacturing such structural components requiring complex design, high mechanical performance, and good surface reactivity [25]. Furthermore, these near-net-shape manufacturing processes tend to limit and even eliminate tooling operations, aiming at considerably reducing processing operations and lead time [26,27]. The powder bed fusion (PBF) AM technique consists in manufacturing parts layer-by-layer by selectively melting thin powder layers using a focused laser or electron source. Such a layered manufacturing strategy, also called “Selective Laser Melting” (SLM), aims to manufacture structural components with both internal and external complex geometries and with spatial resolutions and geometrical tolerances more and more compatible with industrial applications, especially in the field of aerospace. Due to its excellent weldability, SLM-processed Alloy 625 has been widely investigated in terms of solidified microstructure and metallurgical state, crystallographic texture, and mechanical performance in comparison with conventionally wrought Alloy 625 [28–35]. However, the high temperature oxidation resistance of SLM-processed Alloy 625 and coated Alloy 625 components was sparsely reported in the open literature. Fully SLM-processed NiCrAlY coated Alloy 625 was recently investigated in terms of manufacturing feasibility, microstructure, and interdiffusion [36]. A set of optimal processing parameters were identified to produce coatings with very low residual porosity ($\leq 0.1\%$). In addition, contrary to typical overlay NiCrAlY coatings deposited by plasma spray processes, SLM processed NiCrAlY coating exhibited substantial dilution into the Alloy 625 substrate in the as-deposited state, resulting in a progressive Al concentration distribution throughout the coating [36]. The capability of this novel manufacturing approach is promising, and additional microstructural, thermal stability, mechanical performance and surface reactivity characterizations are needed to validate this processing route.

In the present investigation, the high temperature oxidation behavior under isothermal conditions of fully SLM-processed NiCrAlY overlaying Alloy 625 parts is investigated between 800 °C and 1000 °C by means of *ex-situ* thermogravimetric analyses (TGA) in order to document their oxidation kinetics. The oxidation behavior of the coated superalloy is compared to the one of bulk NiCrAlY and Alloy 625. Optical and scanning electron microscopy observations of the sample surface and cross-section, X-ray diffraction, energy dispersive spectroscopy, and topographic analyses were also conducted to document local oxidation events related to the fabrication process.

2. Experimetal procedures

2.1. Materials

Bulk Alloy 625, bulk NiCrAlY and NiCrAlY coated Alloy 625 samples were manufactured by SLM. The Alloy 625 and the NiCrAlY powders, obtained by gas-atomization, were supplied by SLM SOLUTIONS and DUCAL INTERNATIONAL, respectively. The chemical composition of both powders was measured by inductively coupled plasma optical emission spectrometry (ICP-OES) and are reported in Table 1. The average diameters of the powders were similar, *i.e.* 29 µm for the Alloy 625 powder and 35 µm for the NiCrAlY powder. The morphology, the size distribution, and the flow rate of both powders used are detailed in Ref. [36].

A SLM 125HL© machine from SLM SOLUTIONS was used to manufacture the different samples. It is equipped with a 400 W Yb laser (1075 nm) with a Gaussian-beam-focus diameter of 70–100 µm. The fabrication process was performed under a protective argon atmosphere to limit oxidation: the build chamber was initially flooded with argon, then the pressure was kept at 80 mbar during the process. The partial pressure of oxygen was kept below 0.1 atomic %. Furthermore, a constant flow of Ar was maintained above the powder bed to blow away the spatter. The building platform was held at 150 °C (for NiCrAlY) or 200 °C (for Alloy 625) during the whole process to reduce thermal stresses. The different processing conditions and sample geometries used to manufacture the three materials are reported in Table 2 and in Fig. 1. The scanning strategy included contours and used a stripes fill pattern type including stripes with length of 7.5 mm (for NiCrAlY coatings) or 10 mm (for Alloy 625 and bulk NiCrAlY) and a rotation angle of the scanning directions of 67° (for NiCrAlY coatings) or 33° (for Alloy 625 and bulk NiCrAlY) between consecutive layers. A hatch spacing h of 120 µm and a layer thickness t of 50 µm were selected for all the SLM processed materials. These parameters correspond to standard parameters recommended by SLM SOLUTIONS for Alloy 625, and optimized parameters determined in a previous work for NiCrAlY [36].

For bulk Alloy 625, $10 \times 10 \times 10\ mm^3$ samples were manufactured on small pillar and block supports for easier sample removal from the substrate plate (Fig. 1(a)). Note that no stress release heat treatment was applied to the samples. 1-mm thick slices were then extracted from the cube with a precision cutting machine (Isomet5000 from

Table 2
Processing parameters used to manufacture the bulk Alloy 625, the bulk NiCrAlY and the NiCrAlY coated Alloy 625.

	Power P (W)	Scanning speed v ($mm{\cdot}s^{-1}$)	Angle increment (°)	Stripe length (mm)
Bulk In625	275	760	33	10
Bulk NiCrAlY	250	800	33	10
In625 substrate	275	760	33	10
NiCrAlY coating	250	800	67	7.5

Fig. 1. Sample geometry for the three materials: (a) bulk Alloy 625, (b) bulk NiCrAlY, and (c) NiCrAlY coated Alloy 625 samples.

BUEHLER).

For bulk NiCrAlY, 15 × 10 mm^2, 1-mm thick samples were directly fabricated onto the substrate plate (Fig. 1(b)) and samples were then sliced using electrodischarge machining (EDM). A preliminary study aimed to optimize the sample geometry for bulk NiCrAlY samples due to the highly brittle behavior of MCrAlY coating below 600–800 °C [37]. Therefore, bulk NiCrAlY samples had a design with larger dimensions than bulk Alloy 625 ones. Samples were manufactured with rounded corners to avoid severe cracking during the fabrication. Bulk NiCrAlY samples were polished using a precision Jig to gently remove the initial roughness of the sample as well as the potential dilution region affected by the substrate plate. The polishing procedure is detailed in Ref. [38].

For NiCrAlY coated Alloy 625, 5 × 5 × 5 mm^3 Alloy 625 samples were first manufactured on small pillar type supports (Fig. 1(c)). The SLM machine was subsequently cleaned to switch to NiCrAlY powder feed. Then, two layers of NiCrAlY powder (about 100 µm) were SLM processed on the top surface only of the small cubes without any further surface preparation. Based on the apparent density of the powder (around 60%), this would theoretically correspond to a coating layer of about 60-70 µm thick after solidification. Samples were removed from the substrate plate and sliced in the middle plane parallel to the coating surface, leaving a total thickness of about 1 mm, to limit contribution of the coating free side surfaces during oxidation tests. The bottom surface sliced was finally polished all together with the same precision Jig as for bulk NiCrAlY samples to ensure parallelism between the coating surface and the back face as well as repeatability in specimen thickness.

It is worth noting that bulk Alloy 625 and bulk NiCrAlY samples were polished on both faces (P2400 grit paper) while solely the Alloy 625 face for NiCrAlY coated Alloy 625 samples was polished, the coating surface remaining in the as-built ("AB") state from SLM fabrication. Therefore, the true surface of the NiCrAlY coating is thus significantly larger. All the samples were finally subjected to two consecutive heat treatments under vacuum designed for promoting interdiffusion for standard NiCrAlY coated parts: 6 h at 1080 °C followed by 20 h at 870 °C [39]. This metallurgical state was hereafter labelled "as-heat-treated" ("AHT") microstructure in the present paper and is the microstructure of interest in the present study.

It should also be noted that both bulk NiCrAlY and NiCrAlY coatings exhibited some cracks as what is assumed to be the result of delayed cracking caused by high levels of residual stress within the material, a typical feature of SLM processing [40]. Indeed, these cracks appear after some time if no heat treatment is performed quickly after manufacturing, in a time scale not yet determined. If the diffusion heat treatment is performed right after manufacturing by SLM, which is not the case in this study, little to no cracking is expected.

2.2. High temperature oxidation

Isothermal oxidation tests were conducted under laboratory air at 800, 900, and 1000 °C for a maximum duration of 200 h.

Bulk Alloy 625 and NiCrAlY samples were oxidized for 48 h in a SETSYS thermobalance from SETARAM to continuously monitor the mass evolution during the high temperature exposure (resolution of 10 µg). Samples were directly hung in the furnace using a platinum suspension. Samples with dimensions of 10 × 10 × 0.5 and 15 × 10 × 0.5 mm^3 were used for bulk Alloy 625 and for bulk NiCrAlY, respectively. Based on the brittleness of NiCrAlY materials, a 1.5 mm-diameter hole was purposely included in the design produced by SLM. For bulk Alloy 625, the 1.5 mm-diameter hole to hung the sample with the Pt wire was drilled.

For NiCrAlY coated Alloy 625 samples, *ex-situ* thermogravimetric analyses were performed using a NABERTHERM N 11/H furnace, due to the size of samples judged too small for *in-situ* analysis. The temperature was recorded with a K-type thermocouple, and the mass evolution was measured using a precision balance (SARTORIUS MC5) with a resolution of ± 1 µg. Samples were directly hung in an alumina crucible with platinum wires to expose all sample faces to the environment. Interruptions at definite exposure times were carried out, *i.e.* 5, 10, 20, 50, 100, and 200 h to document the evolution of the mass gain and the nature of the oxidation products.

Macrographs of the samples were acquired with a LEICA DMS 300 calibrated microscope in order to measure the projected surface of samples by image analysis, which was subsequently used for the calculation of specific mass gain.

Topographic measurements were conducted using an OLS 5000 LEXT laser scanning confocal microscope by OLYMPUS with a 405 nm monochromatic source and a MPLFLN10xLEXT lens. Height measurement maps of the NiCrAlY coated Alloy 625 samples were acquired with a z-resolution of 0.1 µm and x/y-resolution of 0.3 µm. Topographic measurements were necessary to assess the developed surface of the NiCrAlY coated Alloy 625 samples with their as-built roughness. Stitching reconstruction was used to cover the 5 × 5 mm^2 sample surface. Prior to weighing and oxidation, all samples were cleaned for 15 min in acetone, followed by 15 min in ethanol using a ultrasonic bath.

2.3. Material characterizations

Surface and cross sectional observations were conducted using a field-emission gun scanning electron microscope (FEG-SEM) Nova NanoSEM 450 from THERMOFISHER SCIENTIFIC in a backscattered electron mode. The FEG-SEM was equipped with a GENESIS APEX 2i EDS detector from *EDAX* for chemical profiles and mapping. For cross-sectional characterizations, the samples were hot mounted without cutting to not alter the oxides at the surface of the oxidized samples. The mounted samples were then polished up to the mid-section plane of the specimen using standard automatic metallographic techniques and a surface finish of 0.05 µm alumina particles suspension. An X'PERT PANALYTICAL X-Ray diffractometer from PHILIPS was used for the identification of crystallographic structures. X-ray scans were recorded using the Cu-Kα radiation (λ = 1.54Å), covering a range of angles (2θ) from 15° to 100° with a step size of 0.033°.

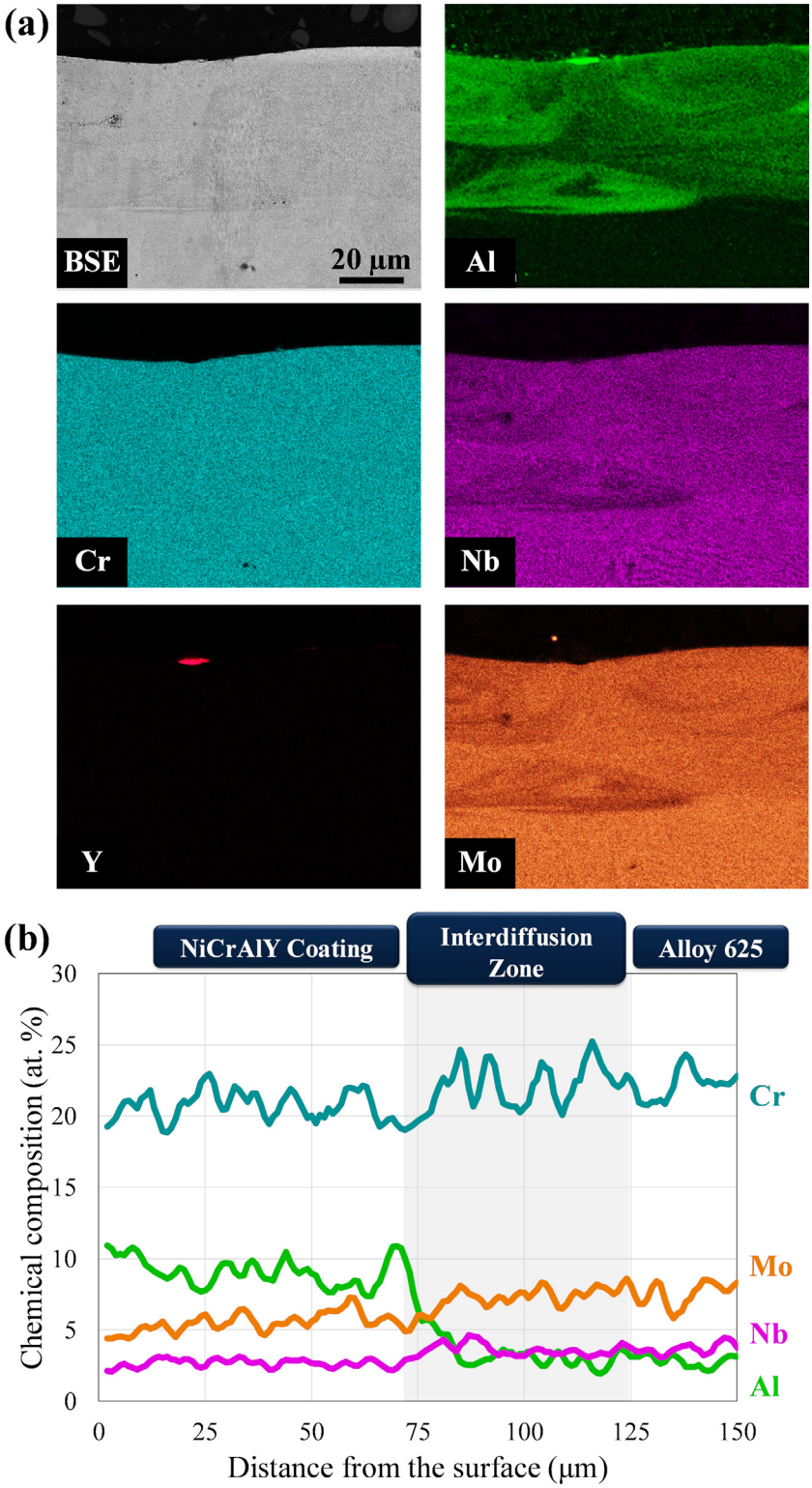

Fig. 2. Element distribution of the NiCrAlY coated Alloy 625 sample before heat treatment (as-built state) measured with EDS: (a) Micrograph in BSE mode and element maps for Al, Cr, Nb, Mo and Y, and (b) Chemical profiles showing the interdiffusion between the NiCrAlY coating and the Alloy 625 substrate.

3. Results

3.1. Chemical analysis of the as-built NiCrAlY coated Alloy 625

Cross-sectional analyses of as-built (AB) NiCrAlY coated Alloy 625 samples, *i.e.* just after the SLM process, were conducted to document the gradient of chemical composition within the coated system due to dilution effects. EDS maps in Fig. 2(a) give a qualitative representation of the element distribution within the 60 µm thick coating in the as-built state (before heat treatment) and Alloy 625 substrate. It highlights the presence of substantial amount of Nb and Mo within the coating as a result of dilution of the coating into the substrate when processing the two layers of NiCrAlY powders by SLM, which typically involves the remelting of already solidified material across several layers. While the

chromium element map is particularly homogeneous along the whole cross-section, a layered/bead pattern is observed for Al, Nb and Mo elements, leading to strong variability in local chemical composition. As expected, the Al content is higher in the coating compared to the bulk Alloy 625, and the Nb and Mo content is slightly lower. The presence of significant amount of alloying elements from the Alloy 625 substrate explains the difference in microstructure with the bulk NiCrAlY variant, notably the precipitation of the Mo-rich σ phase after the heat treatment (Section 3.2). The chemical profiles in Fig. 2(b) aim to further evidence this dilution effect. Al content was found twice higher in the NiCrAlY coating compared to the bulk Alloy 625, showing the Al enrichment suitable for improvement in high temperature oxidation. However, the Al content in the NiCrAlY coating is nearly 40% lower than the one in the NiCrAlY powder and bulk NiCrAlY. Nb and Mo levels in the coating represent about 70% of the content in bulk Alloy 625. Interestingly, the coating region appeared to be almost devoid of Y, which was found to fully segregates on the top surface in the form of monoclinic $Y_4Al_2O_9$ oxide (YAM) as mentioned in Section 3.2 below. In addition, the chemical composition of the NiCrAlY coating was analyzed at different locations of the sample. Some variability in the chemical composition was observed and the composition range for each element was added in Table 1. The chemical composition of bulk Alloy 625 and bulk NiCrAlY materials were also reported in Table 1 for information. Both the bulk materials and their respective powders have a similar chemical composition. Hence, Al evaporation during SLM processing, which can be subjected to this issue, was considered as not significant with the set of parameters used.

Top surface observations of as-built NiCrAlY coated Alloy 625 evidenced regularly spaced oxide beads parallel to the scanning direction (Fig. 3(a)). These oxide beads were located at the inter-beads region, *i.e.* in the area between consecutive weld tracks from the NiCrAlY powder SLM processing. These oxides were identified as $Y_4Al_2O_9$ phase (see Supplementary note 1 in the Supplementary Information file). As on the Y EDS map in Fig. 2(a), a cross sectional observation of the $Y_4Al_2O_9$ bead is illustrated in Fig. 3(a). Bulk SLM processed NiCrAlY samples did not exhibit such a significant Y enrichment on the external surface (Fig. 3(b)). Top surface observations also revealed the presence of a local network of small cracks (yellow arrows in Fig. 3(a)) perpendicular to the scanning direction within the NiCrAlY coating, contrary to bulk NiCrAlY samples. It should yet be noted that few macroscopic cracks were observed in bulk NiCrAlY specimens, as mentioned in Section 2.1.

3.2. Microstructure of the "as-heat-treated" NiCrAlY coating versus bulk Alloy 625 and NiCrAlY

The as-heat-treated (AHT) microstructures of bulk Alloy 625, bulk NiCrAlY and NiCrAlY coated Alloy 625 were characterized using scanning electron microscopy in a backscattered electron mode and EDS analysis (Fig. 4). Punctual EDS analyses, EDS mapping, and XRD analyses were added as Supplementary Information to document phase identification for the three materials.

The microstructure of as-heat-treated Alloy 625 was found typical of SLMed Alloy 625 annealed and aged above 850 °C [35,41,42]. It consisted mainly of a FCC γ-Ni matrix with fine, globular Nb-rich MC primary carbides distributed at the grain boundaries and within grains (sub-micrometer in the latter case), as depicted in Fig. 4(c, f). Secondary phases formed during the 20 h dwell at 870 °C were also observed and include some intra- and intergranular δ-Ni_3Nb needle-like particles and bulky secondary carbides distributed along grain boundaries. Based on their chemical composition ((Mo,Nb)-rich and Si-containing), the latter precipitates are expected to be M_6C rather than $M_{23}C_6$ type carbides, as reported in Refs. [42,44]. In addition, $M_{23}C_6$ becomes less stable than M_6C above 850 °C [45,46].

Cross-sectional micrographs of bulk NiCrAlY and NiCrAlY coatings in the heat-treated state were compared at different magnifications in Fig. 4. Significant differences in terms of phase occurrence and morphology were observed between the coating and the bulk variants (Fig. 4(a, d) *versus* Fig. 4(b, e)). A γ-Ni/γ′-Ni_3Al matrix with well dispersed α-Cr precipitates (bulky and lamellar) and (Ni,Y)-rich intermetallic precipitates were identified in the bulk NiCrAlY variant (Fig. 4(b, e)), consistent with the expected phases for Ni-22Cr-10Al-1Y [47].

The NiCrAlY coating microstructure was composed of intragranular Nb-containing γ′-Ni_3Al precipitates and (Mo,Cr)-rich needle-like precipitates embedded in a γ-Ni matrix (Fig. 4(a, d)). The needle-like precipitates, showing specific orientation with the γ-Ni matrix and a composition rich in (Mo,Cr) and depleted in Ni, were identified as the topologically close packed (TCP) phase σ [42–44]. Grain boundaries were decorated with larger γ′-Ni_3Al precipitates, α-Cr precipitates and Mo-rich blocky precipitates having a similar composition to that of the (Mo,Cr)-rich needle-like precipitates, also identified as the TCP σ phase. At last, contrary to the bulk NiCrAlY variant, no (Ni,Y)-rich intermetallic precipitates were found within the coatings. Instead, yttrium was segregated on the top surface of the coating as $Y_4Al_2O_9$ oxide beads locally found at the boundary between NiCrAlY beads (see Section 3.1, Figs. 2(a) and 3(a)). Qualitative elemental analysis by EDS and XRD results indicated that those oxides were most likely the $Y_4Al_2O_9$ phase, often referred as YAM [48].

3.3. Oxidation behavior: mass gain evolution

Thermogravimetric analyses were conducted for the three AHT material variants at 800, 900, and 1000 °C: (i) *in-situ* TGA for bulk NiCrAlY and bulk Alloy 625, (ii) *ex-situ* TGA for NiCrAlY coated Alloy 625.

Regarding bulk NiCrAlY and bulk Alloy 625 specimens, continuous mass evolution was recorded during 48 h for each temperature, as delineated with solid lines in Fig. 5. Dashed lines continuing experimental measurements correspond to the extrapolation of the mass evolution for each material/temperature condition using a parabolic behavior of high temperature oxidation. The parabolic behavior of the oxidation kinetics was confirmed for both materials in the test time interval of 48 h, as

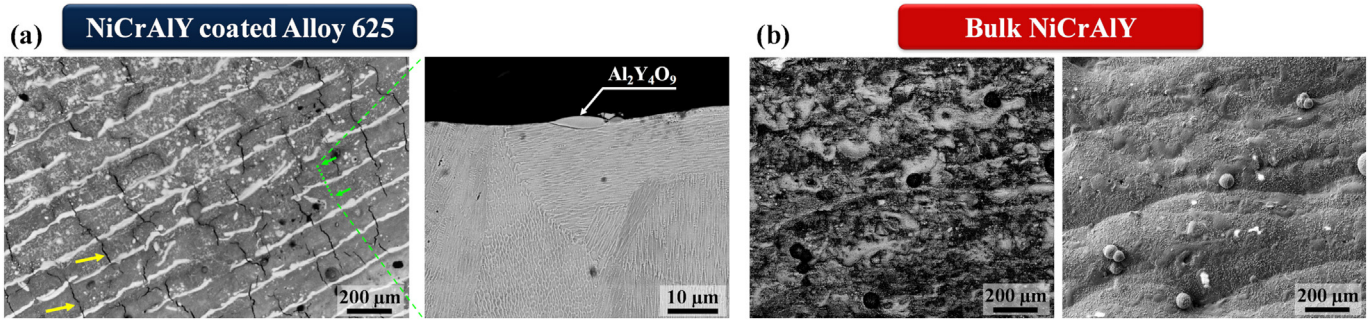

Fig. 3. Segregation in Y for both as-built NiCrAlY materials: (a) NiCrAlY coated Alloy 625, and (b) bulk NiCrAlY.

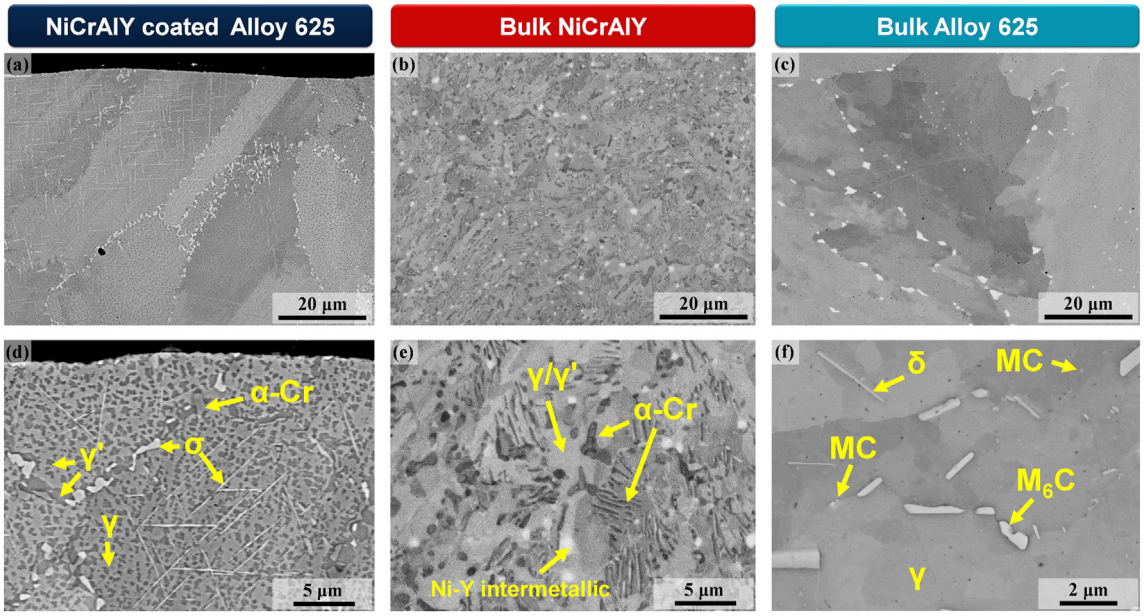

Fig. 4. Cross-sectional observations of the microstructure of the as-heat-treated "AHT" (a, d) NiCrAlY coated Alloy 625, (b, e) bulk NiCrAlY, and (c, f) bulk Alloy 625 samples.

illustrated by the linear trend of the square of the mass gain as a function of the oxidation time in Fig. 6. Parabolic constants k_p for the three temperatures are reported in Table 3 and plotted in an Arrhenius diagram (Fig. 7) with other constants found in the literature for the sake of comparison for bulk materials (different allotropic configurations of Al_2O_3 [22], Cr_2O_3 [49], NiO [50], Alloy 625 [5,9–12], and NiCrAlY alloys [22–24,51,52]). Colored domains in Figs. 5 and 6 correspond to the domain of the square mass gain *vs.* time comprised between the curve of bulk NiCrAlY (lower limit) and bulk Alloy 625 (upper limit) at a given temperature; bulk NiCrAlY exhibits lower kinetics of oxidation than Alloy 625 in the 800-1000 °C temperature window (2.3 times lower at 800 °C and 12.6 times lower at 1000 °C).

Regarding the oxidation behavior of the NiCrAlY coated Alloy 625, it is worth reminding that both bulk NiCrAlY and Alloy 625 specimens were polished then heat-treated under controlled atmosphere (see Section 2.1) prior to oxidation characterization by *in-situ* TGA. In contrast, the topography of the NiCrAlY coatings characterized by *ex-situ* TGA remained in as-built conditions, and thus presented a significantly higher surface roughness compared to the five other polished surfaces of each sample (four lateral and one bottom surfaces). Topographic measurements of the NiCrAlY coatings top surface using laser scanning confocal microscopy were performed on ten specimens. The developed surface, *i.e.* the true surface of the samples, was found to be 1.60 ± 0.13 times larger in average than the projected surface. Therefore, mass gain evolution of the NiCrAlY coated specimens was reported as projected mass gain (Alloy625Coat-Proj) and developed/true mass gain (Alloy625Coat-Dev), *i.e.* taking into account the projected surface of the NiCrAlY coating and the developed/true surface of the NiCrAlY coating, respectively. As for bulk specimens, NiCrAlY coated Alloy 625 samples were heat-treated under a protective

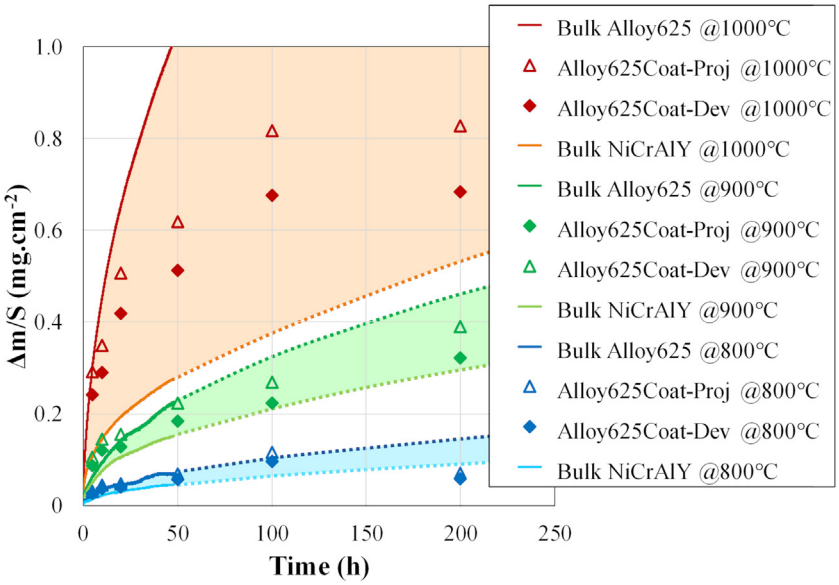

Fig. 5. Mass gain evolution for the three materials at 800 °C, 900 °C and 1000 °C. The measurements of the mass evolution for bulk Alloy 625 and bulk NiCrAlY samples (solid lines) were continuously recorded using a thermobalance and interrupted oxidation tests were conducted for NiCrAlY coated Alloy 625 (data points).

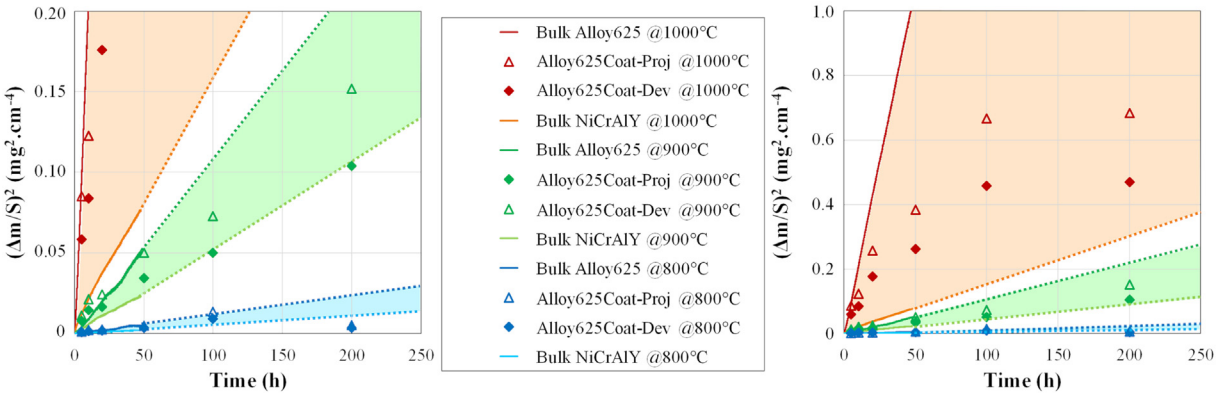

Fig. 6. Evolution of the square mass gain for the three materials at 800 °C, 900 °C and 1000 °C, showing deviation from a parabolic oxidation behavior for NiCrAlY coated Alloy 625 samples.

Table 3
Parabolic constant of oxidation for the bulk Alloy 625, the bulk NiCrAlY and the NiCrAlY coated Alloy 625 (in $mg^2 \cdot cm^{-4} \cdot s^{-1}$).

k_p	Exposure (hours)	800 °C	900 °C	1000 °C
Bulk In625	0–48	$3.01 \cdot 10^{-8}$	$2.81 \cdot 10^{-7}$	$5.92 \cdot 10^{-6}$
Bulk NiCrAlY	0–48	$1.30 \cdot 10^{-8}$	$1.42 \cdot 10^{-7}$	$4.71 \cdot 10^{-7}$
NiCrAlY coated In625 (proj. surf.)	0–50	$2.9 \cdot 10^{-8}$	$2.98 \cdot 10^{-7}$	$2.38 \cdot 10^{-6}$
NiCrAlY coated In625 (proj. surf.)	0–200	$1.41 \cdot 10^{-8}$	$2.14 \cdot 10^{-7}$	$1.20 \cdot 10^{-6}$
NiCrAlY coated In625 (dev. surf.)	0–50	$1.98 \cdot 10^{-8}$	$2.04 \cdot 10^{-7}$	$1.63 \cdot 10^{-6}$
NiCrAlY coated In625 (dev. surf.)	0–200	$9.65 \cdot 10^{-9}$	$1.47 \cdot 10^{-7}$	$8.22 \cdot 10^{-7}$

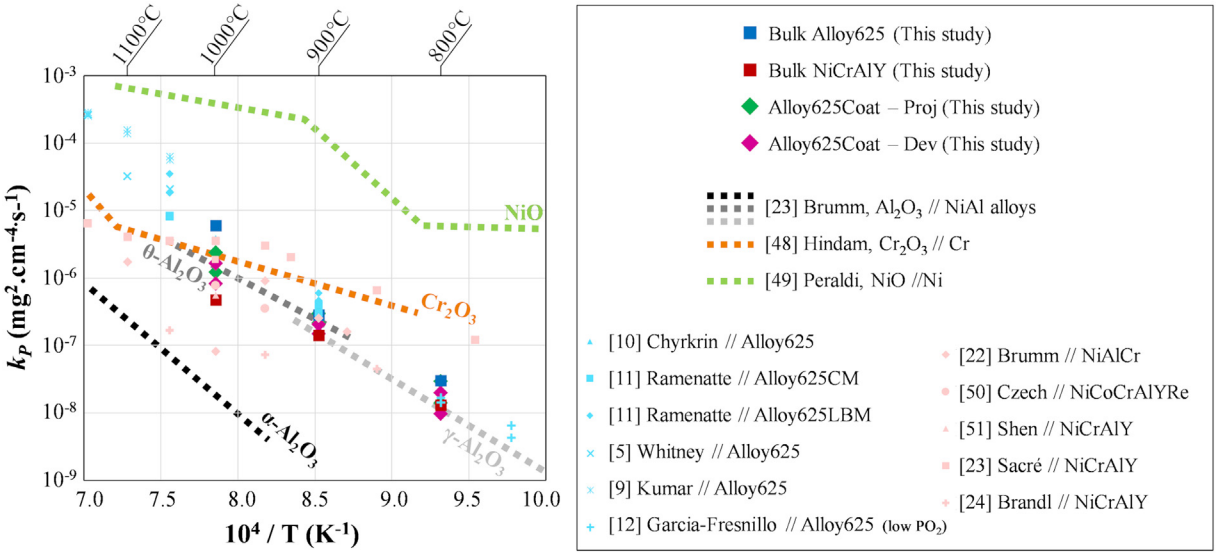

Fig. 7. Evolution of the parabolic constants of oxidation for the three materials as a function of the temperature in comparison with the literature. k_p reported for different allotropic configurations of Al_2O_3 [22], Cr_2O_3 [49], NiO [50], Alloy 625 [5,9–12], and NiCrAlY alloys [22–24, 51, 52]. While the oxidation behavior of both the bulk NiCrAlY and bulk Alloy 625 in the investigated temperature range, the k_p value for NiCrAlY coated Alloy 625 is shown for comparison since its oxidation behavior deviate from a parabolic oxidation behavior.

atmosphere (see Section 2.1), prior to oxidation characterization. Isothermal oxidation tests were conducted at 800, 900, and 1000 °C up to 200 h using one sample per temperature/time condition. Mass gain evolution was reported in Figs. 5 and 6. For most of the oxidation conditions, the oxidation behavior of NiCrAlY coated Alloy 625 is intermediate between that of bulk NiCrAlY and that of bulk Alloy 625 samples. For short time exposures, both the projected and developed mass gains of the bi-material are very similar and sometimes higher than that of the bulk Alloy 625, *i.e.* the upper limit of the corresponding colored oxidation domain. A pronounced mass gain is observed during the transient stage. After a few hours (50 h ≤ t ≤ 100 h), the oxidation behavior of the NiCrAlY coated Alloy 625 deviates from the parabolic regime and tends to follow the behavior of the bulk NiCrAlY samples. In other words, the oxidation behavior of NiCrAlY coated Alloy 625 processed by SLM is not parabolic in this range of temperature (800–1000 °C) and the oxidation kinetics gradually decrease with exposure time. In order to discriminate the oxidation kinetics of the transient oxidation from the long-term oxidation of the NiCrAlY coated Alloy 625 specimens, k_p values between [0 − 50] hours and [0 − 200] hours were calculated and reported in Table 3 and in Fig. 7. k_p values are very close for the three materials at 800 °C but the difference in k_p values increases with the temperature.

3.4. Oxidation behavior: oxidation products

Oxidation products were investigated for the three materials using both EDS and XRD analyses on the top surface and cross-sections of the oxidized specimens (see Supplementary Information). As expected, bulk Alloy 625 developed a continuous, homogeneous and compact Cr_2O_3 external layer for all the temperatures, consistent with the k_p values derived from oxidation tests (Table 3 and Fig. 7). Internal oxidation of Al_2O_3 was observed at the different temperatures. Sparsely distributed NiO oxides and Cr-rich spinels were also observed. In addition, the Cr-depletion beneath the oxide scale promoted the formation of a δ-Ni_3Nb layer beneath the Cr_2O_3 scale, as reported by Chyrkin et al. and Ramenatte et al. [10,11].

For bulk NiCrAlY samples, an external oxide grew on top of the specimen surfaces, mainly constituted of Al_2O_3. Cr_2O_3 was also observed within the external oxide scale, and its proportion, maximal at 800 °C, decreased as temperature increased.

For NiCrAlY coated Alloy 625 samples, the coating free Alloy 625 surfaces behaved similarly to bulk Alloy 625 samples. However, the SLM processed NiCrAlY coating behaved differently from the bulk NiCrAlY samples. Indeed, the oxide scale developing onto the NiCrAlY coating is heterogeneous at all temperatures and exposure times, as illustrated in Fig. 8 showing macrographs of the samples top surface. Most specimens exhibited a bright/medium gray central region surrounded by a darker gray region near the edges, identified by chemical analyses (EDS) on the oxidized surface as respectively constituted of external Al_2O_3 and external Cr_2O_3 oxide scales (Fig. 9). Intermediate gray regions are composed of a mixture of Cr_2O_3/Al_2O_3 external oxides. It is worth noting that the proportion of Cr_2O_3 and Al_2O_3 scale onto the NiCrAlY coating do not correlate to temperature and oxidation duration.

Interestingly, the Y-rich oxides, *i.e.* YAM, observed previously in Fig. 3(a) are intense and distributed continuously along weld tracks in Al_2O_3-rich regions. Cr_2O_3 oxides developed at the cracks present normal to the weld track, as shown in the left Cr element map in Fig. 9. In Cr_2O_3-rich regions, less Y-rich oxides, showing discontinuous distribution, were observed, and no crack within the weld tracks was noticed. Cross-sectional observations of the specimens aimed to identify the presence of internal oxidation (Al_2O_3) beneath the external Cr_2O_3 oxide layer. At 1000 °C–50 h, 15 to 20 μm deep internal oxidation was observed, as illustrated in Fig. 10 showing the microstructure at the junction of bright and dark regions. It is worth noting that the extension of the internal oxidation-affected region increased with temperature and oxidation duration (Fig. 11). For oxidation duration of 100 h, the extension of the internal oxidation affected region was about 4 to 5 μm at 800 °C while the extension was about 18–23 μm at 1000 °C. The platelet-like morphology of the internal Al_2O_3 densified with the time/temperature increase. At 1000 °C, internal Al_2O_3 started coalescing at the internal oxidation front and Al_2O_3-platelets were much thicker in the bulk than in the near-surface region.

3.5. Topography and chemical analyses of the SLM processed NiCrAlY coated specimens

As aforementioned, chemical segregation, heterogeneous crack distribution, and heterogeneous oxide formation were observed on NiCrAlY coated Alloy 625 samples. Large EDS maps were performed on four as-built and as-heat-treated samples to document the element distribution at the top surface of the SLM-processed NiCrAlY coatings. Crack distribution was also estimated from SEM images obtained in secondary electron mode.

Variability in chemical composition was evidenced for all specimens, as illustrated in Fig. 12 for a AHT sample. The back-scattered image of the surface in the AHT state at the upper-left corner clearly shows two regions with different chemical nature: (i) a dark gray central region but also to some extend near the edges, and (ii) a light gray contour in-between. The content of Al, Cr and Y, *i.e.* elements constitutive of the NiCrAlY powder, was higher in the dark gray region than in the bright regions, where elements constitutive of Alloy 625 like Nb and Mo were present in higher proportions (see element maps for the relationship).

Interestingly, cracks, mostly orthogonal to the laser beam direction (direction of the highest tensile residual stress in SLM samples [40]), were concentrated in the Al-rich/dark gray region.

This AHT NiCrAlY coated Alloy 625 was then subjected to 900 °C for 50 h. SEM micrographs obtained in a backscattered electron mode was depicted for the oxidized specimen in Fig. 12 (bottom-right corner). After oxidation, Al_2O_3 external oxide was found to develop solely in the Al- and Cr-rich central region while the periphery was mainly composed of Cr_2O_3 external/Al_2O_3 internal oxides. Some Cr_2O_3 external

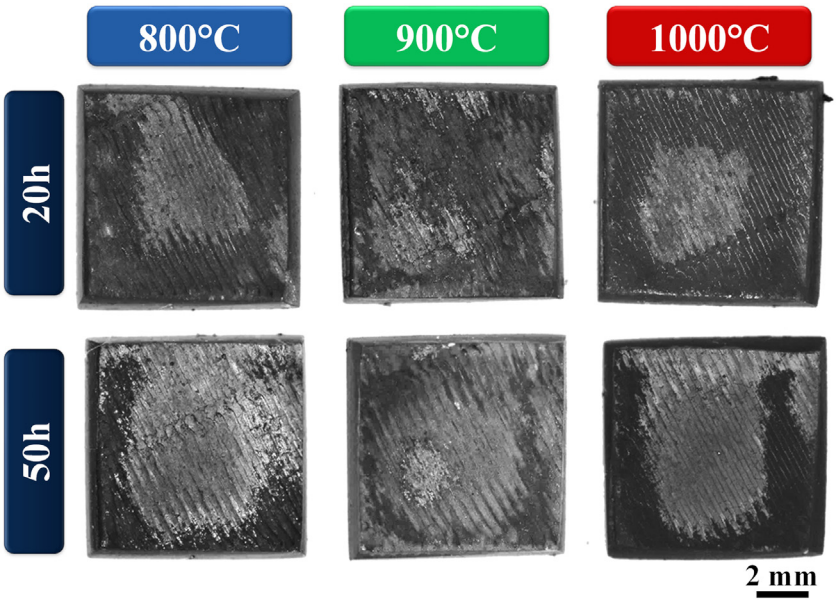

Fig. 8. Surface macrographs of samples oxidized between 800 °C and 1000 °C for 20 and 50 h showing different oxides growing at the surface of the NiCrAlY coated Alloy 625 samples.

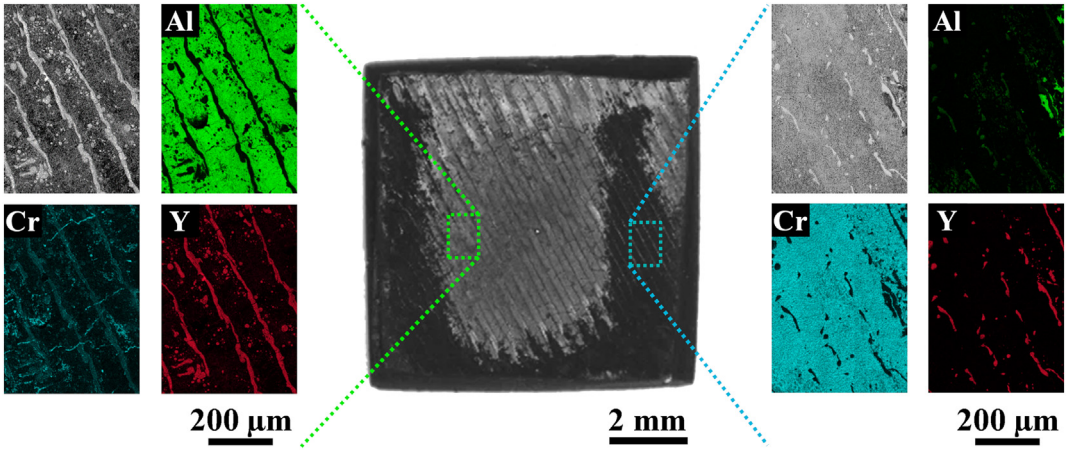

Fig. 9. Formation of Cr_2O_3 and Al_2O_3 external oxides after high temperature exposure (1000 °C - 50 h) at the surface of the NiCrAlY coated Alloy 625 sample.

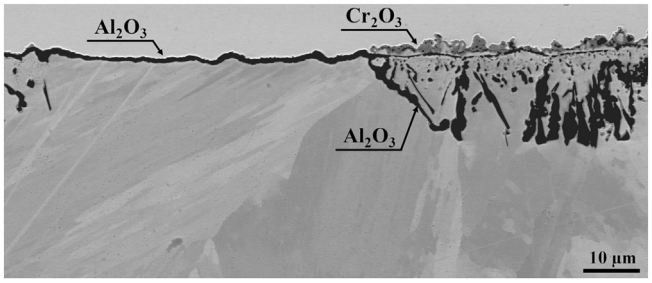

Fig. 10. Cross-section observations of oxidized NiCrAlY coated Alloy 625 samples exposed at 1000 °C for 50 h showing regions with solely external oxidation of Al_2O_3 and regions with external oxidation of Cr_2O_3 and internal oxidation of Al_2O_3.

oxide mixed with the Al_2O_3 external oxide was also found to develop in the Al- and Cr-rich central region but in a lower proportion.

Topographic measurements were performed on this sample to map the height characteristics of the SLM processed NiCrAlY sample (top right corner in Fig. 12). Black/dark violet and yellow/orange regions corresponded to lower altitude and higher altitude regions, denoted "valley" and "hill", respectively. Interestingly, the valley regions appear to match particularly well with the Al-, Y- and Cr-rich regions, *i.e.* corresponding to a composition closer to that of the NiCrAlY powder.

Large field cross-sectional observation of NiCrAlY coated Alloy 625 sample in electron back-scattered mode in Fig. 13 provides a general view of the sub-surface microstructure as a function of the topography (as SLMed state, *i.e.* before heat treatment). The distinction between the substrate and the NiCrAlY coating microstructure was particularly difficult to assess in the hill regions (top left and top right (#2) regions in Fig. 13) as a result of a Mo and Nb content close to that of the Alloy 625 substrate combined with a low Al content compared to the nominal composition of the NiCrAlY powder (chemical profile in region #2). The effective coating thickness deduced from the chemical profile was approximately 40 µm on average. In the valley regions, *i.e.* the central region #1 in Fig. 13, the coating is significantly darker than the substrate due to a higher Al content (twice the content measured in region #2) and a difference in Mo and Nb content more significantly marked with the Alloy 625 substrate (chemical profile in region #2). The average thickness of the coating in the valley region was about 50 µm, slightly larger than in the hill region. Therefore, while an aluminum enrichment is noticed in both regions, the coating in the valley region contained twice as much aluminum as compared to the hill region, extended slightly deeper within the bi-material and also had a thicker interdiffusion zone (light gray domains in chemical profiles). However, the maximum aluminum content measured within the NiCrAlY coating was only about 10 atomic % in the valley region, *i.e.* about half the content in the NiCrAlY powder due to dilution effect during the SLM process.

4. Discussion

The high temperature oxidation behavior of Alloy 625, bulk NiCrAlY and NiCrAlY coated Alloy 625, all produced by the SLM additive manufacturing process, was investigated in the present study. After a standard two-step heat treatment under vacuum designed for promoting interdiffusion (6 h at 1080 °C followed by 20 h at 870 °C), AHT samples were subjected to isothermal oxidation tests at 800, 900, and 1000 °C for a maximum duration of 200 h, during which mass gain was monitored.

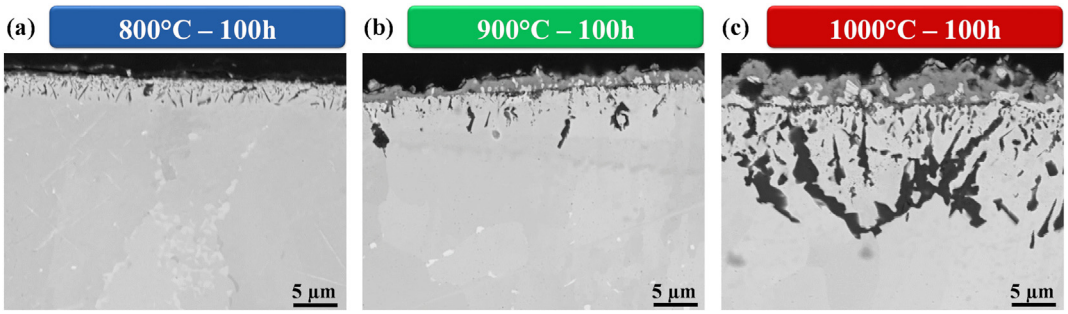

Fig. 11. Cross-section observations of NiCrAlY coated Alloy 625 samples exposed at temperatures between 800 °C and 1000 °C for 100 h showing the extension of the internal oxidation with the temperature.

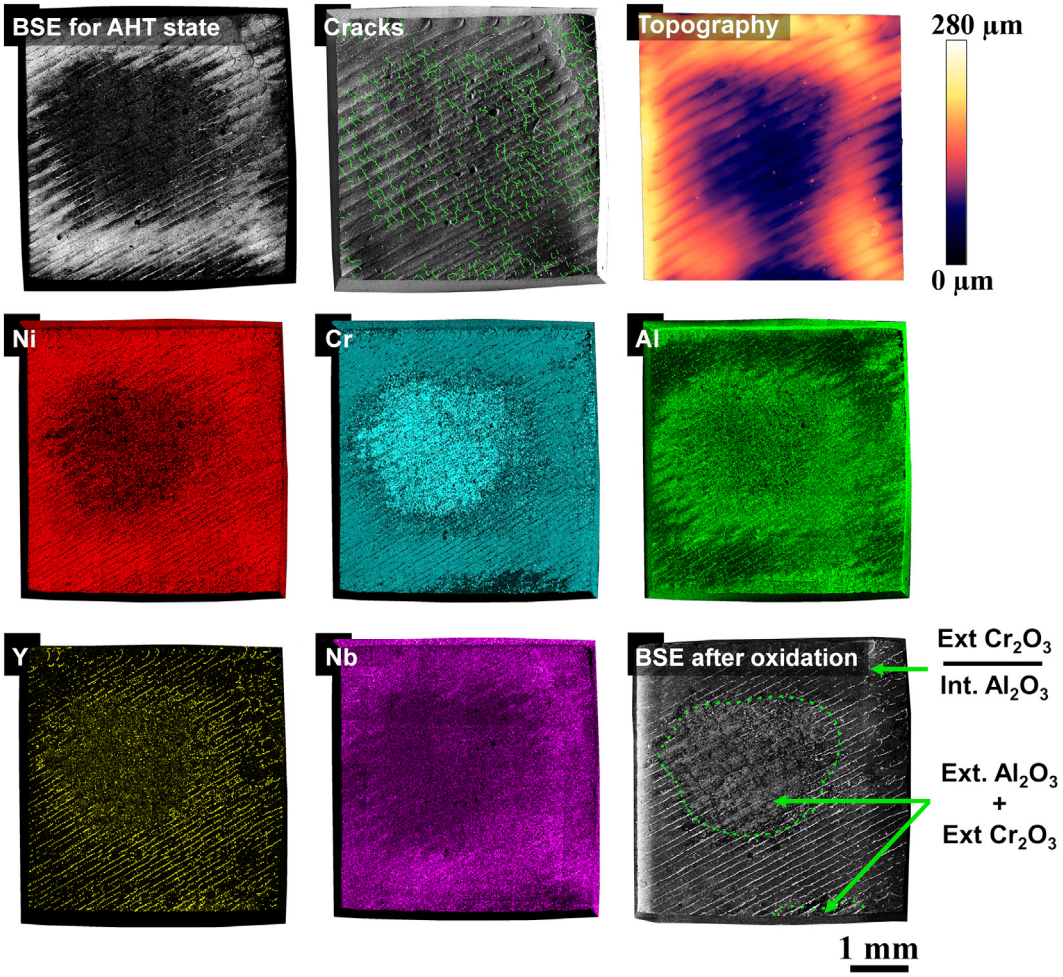

Fig. 12. Effect of the topography and the element distribution at the surface of the NiCrAlY coated Alloy 625 sample on the crack distribution within the coating and the formation of oxides after high temperature exposure. Upper-left corner image is a BSE macrograph of the AHT sample, prior to oxidation.

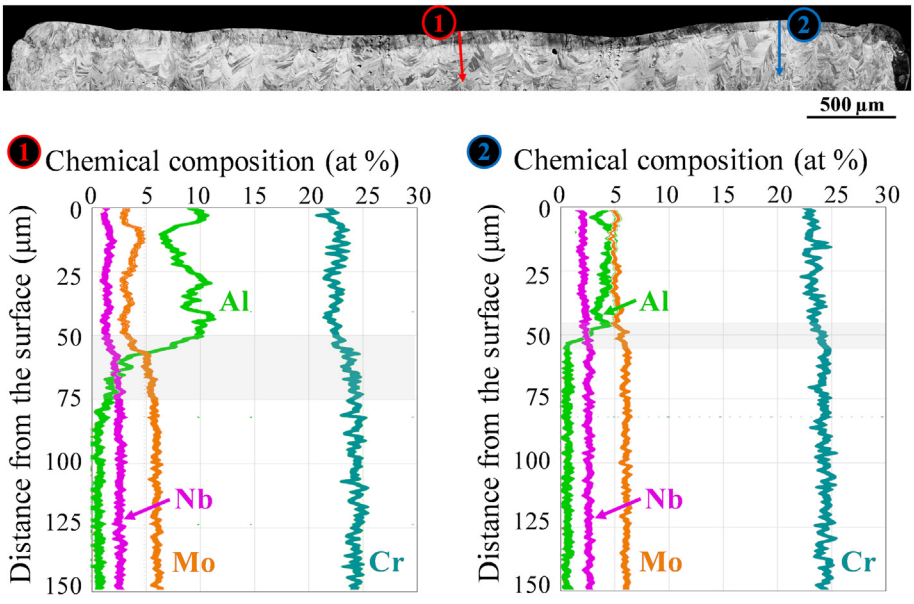

Fig. 13. Microstructure evolution of the as-built NiCrAlY coating, *i.e.* before heat treatment, as a function of the sample topography. Chemical profiles highlighting variability in the SLM processed coating chemistry in valley regions (#1) and hill regions (#2).

4.1. Process-dependant chemistry, microstructure, and oxidation response

While the microstructure and mechanical properties of superalloys produced by SLM have been extensively investigated in the open literature, little work has been done to assess their oxidation behavior at high temperature. As expected, the oxidation of SLMed Alloy 625 was characterized by the growth of a continuous, homogeneous and compact Cr_2O_3 external layer at all temperatures with oxidation kinetics following a parabolic law (Figs. 5 and 6). As shown in Fig. 6 and in Table 3, the derived values of the parabolic constants of oxidation, k_p, ranged from $3.01{\cdot}10^{-8}$ $mg^2{\cdot}cm^{-4}{\cdot}s^{-1}$ at 800 °C to $5.92{\cdot}10^{-6}$ $mg^2{\cdot}cm^{-4}{\cdot}s^{-1}$ at 1000 °C. These k_p values appear comparable and even slightly lower than k_p values for its cast and wrought counterparts [10–12]. However, SLM Alloy 625 demonstrates good performance in high temperature oxidation in the 700–1000 °C range. A frequency factor k_0 of $7.87{\cdot}10^{6}$ $mg^2{\cdot}cm^{-4}{\cdot}s^{-1}$ and $1.68{\cdot}10^{8}$ $mg^2{\cdot}cm^{-4}{\cdot}s^{-1}$ and an activation energy Q of 298 $kJ{\cdot}mol^{-1}$ and 324 $kJ{\cdot}mol^{-1}$ were calculated for the present SLM processed Alloy 625 and for all the oxidation results of Alloy 625 summarized in the Arrhenius plot given in Fig. 7, respectively. It should be noted that oxidation tests were performed on polished, then heat-treated SLMed specimens, which could explain the lower parabolic constants obtained as compared to other studies on additively manufactured Alloy 625. Indeed, a tens-to-hundred-of-nanometer oxide scale developed onto the Alloy 625 specimens during the standard two-step heat treatment despite the vacuum environment, thus slightly lowering the oxidation flux through the oxide scale. Chen et al. [53] reported that the parabolic constant at 1000 °C of heat treated SLMed Alloy 625 was slightly lower than that of as-built samples, possibly due to the fast outward diffusion channels for Cr atoms provided by the dendritic structure composing the microstructure of as-built samples. In addition, AM processes usually produce samples having high surface roughness, which can affect the area of the reactive surface and, therefore, the oxidation properties [11,54–56]. This significant roughness was also reported as a source of deviation from the parabolic oxidation behavior, the mass gain of rough specimens being greater in the early stages of oxidation. This would indeed explain that mass gain is more important at early stage of oxidation for NiCrAlY coated 625 (Figs. 5 and 6).

Standard diffusion heat treatment of the bulk NiCrAlY SLM processed with parameters optimized in a previous study [36] produced the expected γ-Ni/γ′-Ni_3Al + α-Cr microstructure for the chosen composition range (Fig. 4(b, e)). With an aluminum content higher than 10 atomic percent, bulk NiCrAlY promoted the growth of a thin, continuous, slow-growing and adherent Al_2O_3 scale obeying a parabolic law. Cr_2O_3 external oxide mixed with the Al_2O_3 external oxide was also observed, especially at 800 °C. The growth kinetics of the Cr_2O_3 oxide is greater than the Al_2O_3 and participate in an apparent mass gain greater than purely alumina-forming materials. Calculated constants of oxidation k_p ranging from $1.30{\cdot}10^{-8}$ $mg^2{\cdot}cm^{-4}{\cdot}s^{-1}$ at 800 °C to $4.71{\cdot}10^{-7}$ $mg^2{\cdot}cm^{-4}{\cdot}s^{-1}$ at 1000 °C lie within the dispersed range of k_p values for MCrAlY coatings available in the literature [22–24,51,52] and reported in Fig. 7. Constant of oxidation domains for the allotropic variants of Al_2O_3 identified by Brumm et al. [22], *i.e.* α-Al_2O_3, θ-Al_2O_3, and γ-Al_2O_3, reported as dashed black-gray lines in Fig. 7, suggest that the oxide scale formed on the material could be the metastable γ/θ oxide variants, consistent with the relatively low temperature range investigated. However, α-Al_2O_3 was identified with XRD analyses (see Supplementary Information), indicating that metastable alumina could participate in the oxide formation but could transform in α-Al_2O_3 at high temperature exposure.

Fine (Ni,Y)-rich intermetallic precipitates were observed in the bulk NiCrAlY, well dispersed in the microstructure and in a fairly large quantity (Fig. 4(b, d)). Y addition in MCrAlY coatings aims to enhance resistance to oxidation by reactive-element effect [57]. Y is intended to segregate at oxide grain boundaries, to improve the adherence and the protective role of the Al_2O_3 scale by the combination of several mechanisms. Indeed, the formation of Y-rich oxide pegs at the metal/oxide interface [58], the decrease in Al diffusion through Al_2O_3, and the prevention from vacancies coalescence at the metal/oxide interface are highly beneficial in terms of high temperature surface reactivity, especially under thermal cycling [2]. Concentration of reactive element is critical if scale adhesion is to be optimal. Overdoping of the alloy (typically above 0.5% in weight for Y [2]) is known to impair the oxidation resistance of Ni-based alloys through precipitation of Y oxides from Ni-Y intermetallics. The nominal Y content measured within bulk NiCrAlY was close to that of the powder (≈1 wt%). The powder composition was purposely chosen in the present study based on typical composition for plasma spray applications, using powders with a relatively greater content of Y to compensate for significant oxidation during the process. This was not the case during SLM due to the low partial pressure of O_2 within the SLM chamber (≤0.1 wt%) and the protective Ar flow above the powder bed, hence resulting in high Y content within the material. Adjustment of the initial Y concentration in the initial powder would therefore be required to further ensure a more efficient alloy design.

In addition to melting powders, SLM involves the remelting of previously solidified material across several layers, ensuring excellent metallurgical bonding between layers and components with high-density [36]. As a result of manufacturing dissimilar material, and more particularly thin coating, substantial dilution occurs. Effects of this dilution can be observed as deep as hundreds of micrometres, corresponding to typically a thickness of 5 to 10 layers. As observed in the element distribution maps in Fig. 2, the SLM processed NiCrAlY coating onto Alloy 625 contained a significant amount of Mo and Nb. The presence of these two elements results from the remelting of the substrate and the subsequent dilution during the deposition of the two layers of NiCrAlY. Cross section observations showed that although coating thickness was limited to approximately 60 µm, remelted layers went locally as deep as ≈150 µm. Despite good adhesion of the coating and a smoother composition transition at the interface (Figs. 2(b) and 13), the modification of the coated layer composition from the powder composition has three effects: (i) the formation of TCP phases and microstructures after heat treatment very different from that of bulk NiCrAlY (Fig. 4), (ii) the segregation of yttrium at the top surface of the coating as (Y,Al)-rich oxides (Figs. 2 and 3), and (iii) the decrease of the Al content due to dilution (maps of Mo, Nb and Al in Figs. 2 and 13). Regarding the microstructure, the presence of Mo led to the formation of the σ-TCP phase during the heat treatment as intragranular platelet-like precipitates and bulky precipitates at the grain boundaries. The needle-like TCP phases are deleterious in Ni-based superalloys and reported as a potential source for crack initiation and propagation, thus causing low-temperature brittle failure [44]. Nb atoms appeared to have preferentially diffused into γ′ precipitates during the heat treatment, which has the capability to accommodate a small quantity of Nb as a substitute to Al [59].

(Ni-Y)-rich particles were found to precipitate within bulk NiCrAlY whereas YAM oxides ($Y_4Al_2O_9$) solely formed out of the coating, *i.e.* onto the coating top surface. Since bulk NiCrAlY is free of alien Alloy 625 elements, the mechanism leading to Y segregation onto the top surface of the NiCrAlY coating variant is assumed to be as follow: the substantial presence of elements from Alloy 625 within the melt pool, presumably both Mo and Nb, led to a significant drop in the solubility of Y in the alloy. Upon solidification, the liquid phase at the surface of the melt-pool got progressively enriched in Y. Its high reactivity potentially led to the formation of (Al,Y)-rich oxides from the remaining traces of O_2 within the chamber (≤0.1%), identified as $Y_4Al_2O_9$. Upon remelting of the solidified material (adjacent line scan of the same layer or next layer), the less dense oxide remains at the surface of the melt pool as a slag. Surface tension rejects the slag to the side between weld tracks, forming the regularly spaced continuous oxide beads parallel to the scanning direction observed at the top surface of NiCrAlY coated Alloy 625 samples (Figs. 3(a) and 9). This scenario, if confirmed, would make

difficult the addition of reactive Y in SLM processed coatings with thickness smaller than the remelting depth (≈3 to 4 layers), as it would not be possible to avoid a large dilution of the coating powder within the underlaying substrate.

Macrographs of oxidized specimens (Fig. 8), surface element distribution maps (Fig. 12), cross-section observations of the coating (Fig. 13) and surface topography (Fig. 12) evidenced a good correlation between the coating topography, the heterogeneous distribution of Al within the coating and the distribution of oxidation products after exposure to 800 °C, 900 °C and 1000 °C for up to 200 h. As illustrated in the topography map (top right corner in Fig. 12) and the cross-section microstructure in Fig. 13, the coating follows the topography inherited from the manufacturing of the Alloy 625 substrate, which exhibits large hill and valley regions with height difference as high as 180 ± 20 μm on average. Additive manufactured components usually present edges with a higher altitude than the central region for various reasons including (i) the effect of contour scanning strategies in SLM process, (ii) the distortion at free edges, and (iii) the starting/ending points of beads. Given the small surface of the samples (5 × 5 mm), edge effects impact a significant portion of the whole surface. In the default strip scanning strategy used for SLM processing, the whole surface of the building area was divided into 7.5 mm wide stripes and specimens were lased one by one according to the global stripe pattern. When occasionally samples were located between two or more adjacent stripes, the junction would also lead to a visible local variation of the topography (*e.g.* top right sample in Fig. 8). Variations of the substrate topography caused valley regions (mainly central regions) to be covered by a thicker layer of NiCrAlY powder than hill regions (mainly near the edges) during SLM process. The quantity of Al in central regions remained sufficiently high (≈10 at%) to allow the formation a continuous, protective film of external Al_2O_3 (Type III oxidation), as expected from the NiCrAlY coating [19–21]. However, in regions of higher altitude, the thinner coating subject to a higher degree of dilution, led to lower Al content, below the required threshold for an external Al_2O_3 to form. Instead, Type II oxidation behavior typical of high Cr low Al alloys was observed [19–21], characterized by the growth of an external Cr_2O_3 scale and an internal oxidation of Al_2O_3 (Figs. 10 and 11).

The mass gain evolution of NiCrAlY coated Alloy 625, intermediate between those of Al_2O_3-forming bulk NiCrAlY and Cr_2O_3-forming bulk Alloy 625, confirmed that the coating provided some degree of protection towards high temperature oxidation to the substrate, despite the imperfect Al_2O_3 covering of the NiCrAlY coated surface. Contrary to bulk NiCrAlY specimens, the oxidation behavior after few hours of the NiCrAlY coated Alloy 625 deviates from the parabolic regime and tends to the behavior of the bulky NiCrAlY samples. In other words, the oxidation behavior of NiCrAlY coated Alloy 625 processed by SLM is not parabolic in the investigated range of temperature, the oxidation kinetics gradually decreasing with the time. Such deviation from the parabolic oxidation behavior was also observed for an In718 SLM processed oxidized at 850 °C [54–56]. Rough surfaces demonstrate a greater mass gain in the early stages of oxidation then decreasing down to kinetics of polished surface due to surface smoothing and local variation in oxide thickness, oxide in the valley regions being thicker compared to hill regions. It should also be noted that the fraction of Al_2O_3 and Cr_2O_3 growing regions differed from one sample to another (Fig. 8), which could also have contributed to a dispersion of the data (each one corresponding to a different sample).

4.2. Some keys for further improvements

The present study showed that improvement of the high temperature oxidation properties of Alloy 625 between 800 and 1000 °C is possible using a SLM processed NiCrAlY coating. Compared to standard plasma spray deposition, the remelting of the underlaying solidified layers ensures a strong metallurgical bonding of the coating with the substrate and liquid state dilution leads to a smooth composition transition at the interface. Both effects could favour a good adherence of the coating over the lifetime of coated parts. Due to the low pressure of O_2 and the argon shielding flow on top of the powder bed, the SLM process produced coatings devoid of embedded oxidation products. However, several process related issues were noted, which allowed to identify some keys for further improvement in terms of process, chemistry and microstructure. The most striking issue encountered was the heterogeneous distribution of Al element in the coating (in the x-y plane) due to the lack of flatness of the SLM Alloy 625 substrate, enhanced by the small surface area of the samples (edge effects) and the default non-optimized stripe scanning pattern. This issue can be possibly solved by surface preparation of substrates to correct roughness and flatness and/or a wiser selection of scanning strategies and process parameters. For instance, Mohammadian et al. [60] developed a chemical-abrasive flow polishing technical to improve surface finish control of additively-manufactured Alloy 625 components with complex geometries. Note that coating deposition onto flat surfaces only and with relatively small dimension remains a current limitation of the SLM process itself.

The substantial diffusion of Mo and Nb was found to cause heterogeneous segregation to the surface of most of the reactive Y as oxides, where its beneficial effect on the resistance to oxidation would be nullified. Process parameters used in the present study induced deep remelting of the substrate (100–150 μm) relative to the thickness of the NiCrAlY coating. Influence of the substrate in terms of composition alteration in SLM are typically of the order of 200–300 μm, depending on the energy density applied (P, V and hatch distance h). NiCrAlY coatings exceeding 300 μm in thickness are less likely be completely affected by this issue. In the case of thin coatings, adjusting the process parameters for limiting the dilution effect, could be appropriated. At last, addition of reactive element in a different form, as dispersed oxide for example, could also be an alternative strategy.

The modification of coating composition led to changes in the phases present in the microstructure and their morphology, in particular the precipitation of platelet-like and undesirable TCP σ phases in Mo-rich regions after the heat treatment, known to embrittle Ni-based superalloys. The current results did not show evidence of detrimental effects of the σ phase or the modified microstructure other than the particular change in oxidation behavior when the amount of Al dropped below the critical level required for the formation of external Al_2O_3. Strategies for reducing dilution of coatings within the surface such as presented in the previous paragraph, are expected to help promoting a microstructure closer to the one of bulk SLMed NiCrAlY.

Finally, SLM processed coatings presented, as soon as from the as-built stage, a surface network of fine, microscopic cracks within beads, normal to the scanning direction (Fig. 12) and propagating across the whole coatings. These cracks can be very detrimental to the oxidation resistance. The occurrence of high tensile stresses within beads is typical of SLMed materials, stress being maximum along the bead length [40]. Most of the cracks appeared in Al-rich areas of the coatings, where the composition was closer to that of the NiCrAlY composition. Not observed at this scale in bulk NiCrAlY samples, the crack network formed within the thin coating is believed to originate from the higher level of residual stresses within the coating caused by the presence of the underlying Alloy 625 (thermal expansion mismatch, high temperature mechanical performance, *etc.*). Compared to Alloy 625 substrate, NiCrAlY coating has a high amount of Al. Thus, during SLM of NiCrAlY coating onto Alloy 625, the coated NiCrAlY should tend to significantly shrink due to γ′ prime precipitation. However, the Alloy 625 substrate constrained its shrinkage. Accordingly, the coated NiCrAlY is subjected to high degree of tensile stresses. However, it must be noted that the crack network in NiCrAlY coatings occurred as delayed cracking. Preliminary results demonstrated that heat-treating samples consecutively after manufacturing greatly reduces the extend of cracking. A stress relieving heat treatment is advised and often

carried out right after fabrication in typical applications. In the present work, samples were heat treated several weeks after being manufactured, *i.e.* after the occurrence of a large crack network.

5. Conclusions

The main conclusions drawn from this study on the high temperature oxidation in the temperature range of 800 to 1000 °C of a NiCrAlY coating Alloy 625 processed by SLM are given below:

(i) Improvement in high temperature oxidation properties of SLM processed Alloy 625 between 800 and 1000 °C was found possible using a SLM processed NiCrAlY coating, *i.e.* a two-step SLM deposition process;
(ii) Dilution effects due to some remelting of the substrate influence the chemistry and the microstructure of the coating. Using two deposition layers, the aluminum content within the coating was half the content of the NiCrAlY powder composition, and the coating was significantly enriched in elements from the Alloy 625 substrate (Mo and Nb), leading to the segregation of the reactive Y to the surface as $Y_4Al_2O_9$ oxides;
(iii) Dilution effects during the NiCrAlY coating manufacturing was sensitive to the topography of the SLM processed Alloy 625 substrates: thicker powder layers before laser melting in valley region led to elements of the NiCrAlY being more concentrated in the valley regions;
(iv) Variability in oxidation products at the surface of the SLM processed NiCrAlY coating was intimately related to topography-assisted chemical and microstructural heterogeneities;
(v) SLM processed bulk Alloy 625 and bulk NiCrAlY followed a parabolic oxidation behavior in the present temperature range, which was not the case for the NiCrAlY coated Alloy 625 bi-material.

CRediT authorship contribution statement

Damien Texier:Conceptualization, Methodology, Data curation, Validation, Investigation, Writing - original draft, Writing - review & editing, Visualization.**Etienne Copin**:Conceptualization, Methodology, Data curation, Validation, Investigation, Funding acquisition, Writing - original draft, Writing - review & editing, Visualization.**Agustin Flores**:Methodology, Data curation, Investigation, Writing - original draft, Visualization.**Jiwon Lee**:Methodology, Investigation, Writing - review & editing, Visualization.**Mathieu Terner**:Conceptualization, Methodology, Validation, Funding acquisition, Writing - original draft, Writing - review & editing, Visualization.**Hyun-Uk Hong**:Conceptualization, Supervision, Funding acquisition, Project administration, Writing - review & editing.**Philippe Lours**:Conceptualization, Supervision, Funding acquisition, Project administration, Writing - review & editing.

Declaration of competing interest

The authors declare that they have no known competing financial interests or personal relationships that could have appeared to influence the work reported in this paper.

Acknowledgements

The authors acknowledge the financial support of the National Research Foundation of Korea (NRF) grant funded by the Korean government (MSIP, NRF-2020R1A2C4002291 and NRF-2018R1A5A6075959). This work used the precision Jig for specimen preparation developed during the ANR-JCJC-COMPAACT project funded by the Agence Nationale de la Recherche (ANR) [ANR-18-CE08-0003]. The authors are grateful to the Raimond Castaing Microanalysis Centre (Mixed Services Unit 3623) for access to microscopy facilities.

Appendix A. Supplementary data

Supplementary data to this article can be found online at https://doi.org/10.1016/j.surfcoat.2020.126041.

References

[1] T. Pollock, S. Tin, Nickel-based superalloys for advanced turbine engines: chemistry, microstructure, and properties, J. Propuls. Power 22 (2006) 361–374.
[2] R. Reed, The Superalloys: Fundamentals and Applications, Cambridge University Press, 2008.
[3] D.J. Young, High Temperature Oxidation and Corrosion of Metals, 2nd ed., Elsevier Science, 2016, https://doi.org/10.1016/B978-0-08-100101-1.01001-3.
[4] C. Vernot-Loier, F. Cortial, Influence of heat treatments on microstructure, Mechanical Properties and Corrosion Behaviour of Alloy 625 Forged Rod (2012) 409–422.
[5] E. Whitney, G. Smikovich, J. Fink, High Temperature Oxidation of a Modified Alloy 625 (2012) 695–704.
[6] H. Eiselstein, D. Tillack, The Invention and Definition of Alloy 625 (2012) 1–14.
[7] L. Mataveli Suave, D. Bertheau, J. Cormier, P. Villechaise, A. Soula, Z. Hervier, F. Hamon, J. Laigo, Impact of thermomechanical aging on alloy 625 high temperature mechanical properties, 8th International Symposium on Superalloy 718 and Derivatives, 2014 2014, pp. 317–331.
[8] L. Mataveli Suave, J. Cormier, D. Bertheau, P. Villechaise, A. Soula, Z. Hervier, F. Hamon, High temperature low cycle fatigue properties of alloy 625, Mater. Sci. Eng. A 650 (2016) 161–170.
[9] L. Kumar, R. Venkataramani, M. Sundararaman, P. Mukhopadhyay, S.P. Garg, Studies on the oxidation behavior of inconel 625 between 873 and 1523 K, Oxid. Met. 45 (1996) 221–244.
[10] A. Chyrkin, P. Huczkowski, V. Shemet, L. Singheiser, W.J. Quadakkers, Sub-scale depletion and enrichment processes during high temperature oxidation of the nickel base alloy 625 in the temperature range 900–1000°C, Oxid. Met. 75 (2011) 143–166.
[11] N. Ramenatte, A. Vernouillet, S. Mathieu, A. Vande Put, M. Vilasi, D. Monceau, A comparison of the high-temperature oxidation behaviour of conventional wrought and laser beam melted Inconel 625, Corros. Sci. 164 (2020) 108347.
[12] L. Garcia-Fresnillo, A. Chyrkin, C. Böhme, J. Barnikel, F. Schmitz, W. Quadakkers, Oxidation behaviour and microstructural stability of alloy 625 during long-term exposure in steam, J. Mater. Sci. 49 (2014) 6127–6142.
[13] C.S. Tedmon, The effect of oxide volatilization on the oxidation kinetics of cr and fe-cr alloys, J. Electrochem. Soc. 113 (1966) 766.
[14] D. Young, B. Pint, Chromium volatilization rates from Cr2O3 scales into flowing gases containing water vapor, Oxid. Met. 66 (2006) 137–153.
[15] R. Mévrel, State of the art on high-temperature corrosion-resistant coatings, Mater. Sci. Eng. A 120–121 (1989) 13–24.
[16] T. Rhys-Jones, Coatings for Blade and Vane Applications in Gas Turbines, (1989), https://doi.org/10.1016/0010-938X(89)90104-2.
[17] S. Bose, High Temperature Coatings, 1st ed., 81 Butterworth-Heinemann, 2007, https://doi.org/10.1007/s11085-013-9462-3.
[18] W. Leng, R. Pillai, P. Huczkowski, D. Naumenko, W. Quadakkers, Microstructural evolution of an aluminide coating on alloy 625 during wet air exposure at 900 °C and 1000 °C, Surf. Coat. Technol. 354 (2018) 268–280.
[19] G. Wallwork, A. Hed, Some limiting factors in the use of alloys at high temperatures, Oxid. Met. 3 (1971) 171–184.
[20] C. Giggins, F. Pettit, Oxidation of Ni-Cr-Al alloys between 1000° and 1200°C, J. Electrochem. Soc. 118 (1971) 1782–1790.
[21] J. Smialek, N. Jacobson, Oxidation of high-temperature aerospace materials, in: Y. Bar-Cohen (Ed.), High Temperature Materials and Mechanisms, February, 2014, pp. 95–162, , https://doi.org/10.1201/b16545-6.
[22] M. Brumm, H. Grabke, The oxidation behaviour of NiAl-I. Phase transformations in the alumina scale during oxidation of NiAl and NiAl-Cr alloys, Corros. Sci. 33 (1992) 1677–1690.
[23] S. Sacré, U. Wienstroth, H. Feller, L. Thomas, Influence of the phase compositions on the transient-stage high-temperature oxidation behaviour of an NiCoCrAlY coating material, J. Mater. Sci. 28 (1993) 1843–1848.
[24] W. Brandl, D. Toma, H. Grabke, The characteristics of alumina scales formed on HVOF-sprayed MCrAlY coatings, Surf. Coat. Technol. 108–109 (1998) 10–15.
[25] T. DebRoy, H. Wei, J. Zuback, T. Mukherjee, J. Elmer, J. Milewski, A. Beese, A. Wilson-Heid, Z.W. De A, Additive manufacturing of metallic components – process, structure and properties, Prog. Mater. Sci. 92 (2018) 112–224.
[26] W.E. Frazier, Metal additive manufacturing: a review, J. Mater. Eng. Perform. 23 (2014) 1917–1928.
[27] K. Wong, A. Hernandez, A review of additive manufacturing, ISRN Mechanical Engineering (2012) 1.
[28] D. Ma, A.D. Stoica, Z. Wang, A.M. Beese, Crystallographic texture in an additively manufactured nickel-base superalloy, Mater. Sci. Eng. A 684 (2017) 47–53.
[29] G. Lindwall, C.E. Campbell, E.A. Lass, F. Zhang, M.R. Stoudt, A.J. Allen, L.E. Levine, Simulation of TTT curves for additively manufactured inconel 625, Metallurgical

and Materials Transactions A: Physical Metallurgy and Materials Science 50 (2019) 457–467.
[30] A. Kreitcberg, V. Brailovski, S. Turenne, Elevated temperature mechanical behavior of IN625 alloy processed by laser powder-bed fusion, Mater. Sci. Eng. A 700 (2017) 540–553.
[31] I. Koutiri, E. Pessard, P. Peyre, O. Amlou, T. De Terris, Influence of SLM process parameters on the surface finish, porosity rate and fatigue behavior of as-built Inconel 625 parts, J. Mater. Process. Technol. 255 (2018) 536–546.
[32] S. Li, Q. Wei, Y. Shi, C.K. Chua, Z. Zhu, D. Zhang, Microstructure characteristics of Inconel 625 superalloy manufactured by selective laser melting, J. Mater. Sci. Technol. 31 (2015) 946–952.
[33] M. Leary, M. Mazur, H. Williams, E. Yang, A. Alghamdi, B. Lozanovski, X. Zhang, D. Shidid, L. Farahbod-Sternahl, G. Witt, I. Kelbassa, P. Choong, M. Qian, M. Brandt, Inconel 625 lattice structures manufactured by selective laser melting (SLM): mechanical properties, deformation and failure modes, Mater. Des. 157 (2018) 179–199.
[34] C. Li, R. White, X.Y. Fang, M. Weaver, Y.B. Guo, Microstructure evolution characteristics of Inconel 625 alloy from selective laser melting to heat treatment, Mater. Sci. Eng. A 705 (2017) 20–31.
[35] G. Marchese, M. Lorusso, S. Parizia, E. Bassini, J.-W. Lee, F. Calignano, D. Manfredi, M. Terne, H.-U. Hong, D. Ugues, M. Lombardi, S. Biamino, Influence of heat treatments on microstructure evolution and mechanical properties of Inconel 625 processed by laser powder bed fusion, Mater. Sci. Eng. A 729 (2018) 64–75.
[36] J. Lee, M. Terner, E. Copin, P. Lours, H.U. Hong, A novel approach to the production of NiCrAlY bond coat onto IN625 superalloy by selective laser melting, Additive Manufacturing 31 (2020) 100998.
[37] D. Texier, D. Monceau, F. Crabos, E. Andrieu, Tensile properties of a non-line-of-sight processed $\beta - \gamma - \gamma'$ MCrAlY coating at high temperature, Surf. Coat. Technol. 326 (2017) 28–36.
[38] D. Texier, D. Monceau, J.-C. Salabura, R. Mainguy, E. Andrieu, Micromechanical testing of ultrathin layered material specimens at elevated temperature, Mater. High Temp. 33 (2016) 325–337.
[39] D. Texier, D. Monceau, Z. Hervier, E. Andrieu, Effect of interdiffusion on mechanical and thermal expansion properties at high temperature of a MCrAlY coated Ni-based superalloy, Surf. Coat. Technol. 307 ((2016) 81–90.
[40] S. Le Roux, M. Salem, A. Hor, Improvement of the bridge curvature method to assess residual stresses in selective laser melting, Additive Manufacturing 22 (2018) 320–329.
[41] Z. Tian, C. Zhang, D. Wang, W. Liu, X. Fang, D. Wellmann, Y. Zhao, Y. Tian, A review on laser powder bed fusion of Inconel 625 nickel-based alloy, Appl. Sci. 10 (2020) 81.
[42] L. Mataveli Suave, J. Cormier, P. Villechaise, A. Soula, Z. Hervier, D. Bertheau, J. Laigo, Microstructural evolutions during thermal aging of alloy 625: impact of temperature and forming process, Metall. Mater. Trans. A 45 (2014) 2963–2982.
[43] J. Davis, ASM Specialty Handbook: Nickel, Cobalt, and their Alloys, ASM International, 2000.
[44] C. Sims, N. Stoloff, W. Hagel, Superalloys II: High-Temperature Materials for Aerospace and Industrial Power, 2nd ed., Wiley, 1987.
[45] N. Evans, P. Maziasz, J. Shingledecker, Y. Yamamoto, Microstructure evolution of alloy 625 foil and sheet during creep at 750 °C, Mater. Sci. Eng. A 498 (2008) 412–420.
[46] M. Donachie, S. Donachie, Superalloys: A Technical Guide, 2nd ed., ASM International, 2002.
[47] M.T. Pace, R.C. Thomson, J. Wells, Oxidation of MCrAlY coatings on Ni based superalloys, Energy Materials 2 (2007) 181–190.
[48] O. Fabrichnaya, H.J. Seifert, R. Weiland, T. Ludwig, F. Aldinger, A. Navrotsky, Phase equilibria and thermodynamics in the Y_2O_3-Al_2O_3-SiO_2 system, Z. Met. 92 (2001) 1083–1097.
[49] H. Hindam, D. Whittle, Microstructure, adhesion and growth kinetics of protective scales on metals and alloys, Oxid. Met. 18 (1982) 245–284.
[50] R. Peraldi, D. Monceau, B. Pieraggi, Evolution of scale microstructure as a function of scale oxide thickness during oxidation of nickel at 700°C, Mater. Sci. Forum 369–372 (2001) 189–196.
[51] N. Czech, M. Juez-Lorenzo, V. Kolarik, W. Stamm, Influence of the surface roughness on the oxide scale formation on MCrAlY coatings studied in situ by high temperature X-ray diffraction, Surf. Coat. Technol. 108–109 (1998) 36–42.
[52] M. Shen, P. Zhao, Y. Gu, S. Zhu, F. Wang, High vacuum arc ion plating NiCrAlY coatings: microstructure and oxidation behavior, Corros. Sci. 94 (2015) 294–304.
[53] L. Chen, Y. Sun, L. Li, X. Ren, Effect of heat treatment on the microstructure and high temperature oxidation behavior of TiC/Inconel 625 nanocomposites fabricated by selective laser melting, Corros. Sci. 169 (2020) 108606, https://doi.org/10.1016/j.corsci.2020.108606 (In press).
[54] T. Sanviemvongsak, D. Monceau, B. Macquaire, High temperature oxidation of IN 718 manufactured by laser beam melting and electron beam melting: effect of surface topography, Corros. Sci. 141 (2018) 127–145.
[55] D. Seo, K. Ogawa, T. Shoji, S. Murata, High-temperature oxidation behavior and surface roughness evolution of VPS NiCrAlY coating, J. Therm. Spray Technol. 17 (2008) 136–143.
[56] L.-y. Ni, Z.-l. Wu, C.-g. Zhou, Effects of surface modification on isothermal oxidation behavior of HVOF-sprayed NiCrAlY coatings, Progress in Natural Science: Materials International 21 (2011) 173–179.
[57] D.P. Whittle, J. Stringer, Improvements in high-temperature oxidation resistance by additions of reactive elements or oxide dispersions, Philos. Trans. R. Soc. Lond. 295A (1980) 309–329.
[58] H. Tawancy, N. Abbas, A. Bennett, Role of Y during high temperature oxidation of an M-Cr-Al-Y coating on an Ni-base superalloy, Surf. Coat. Technol. 68–69 (1994) 10–16.
[59] W. Mankins, S. Lamb, Nickel and Nickel Alloys, ASM International, 1990, https://doi.org/10.31399/asm.hb.v02.9781627081627.
[60] N. Mohammadian, S. Turenne, V. Brailovski, Surface finish control of additively-manufactured Inconel 625 components using combined chemical-abrasive flow polishing, J. Mater. Process. Technol. 252 (2018) 728–738.